ARTICLES
PUBLISHED ONLINE: 7 MARCH 2010 | DOI: 10.1038/NNANO.2010.24
nature nanotechnology

Detection of single-molecule H_2O_2 signalling from epidermal growth factor receptor using fluorescent single-walled carbon nanotubes

Hong Jin[1], Daniel A. Heller[1], Marie Kalbacova[2], Jong-Ho Kim[1], Jingqing Zhang[1], Ardemis A. Boghossian[1], Narendra Maheshri[1] and Michael S. Strano[1]*

An emerging concept in cell signalling is the natural role of reactive oxygen species such as hydrogen peroxide (H_2O_2) as beneficial messengers in redox signalling pathways. The nature of H_2O_2 signalling is confounded, however, by difficulties in tracking it in living systems, both spatially and temporally, at low concentrations. Here, we develop an array of fluorescent single-walled carbon nanotubes that can selectively record, in real time, the discrete, stochastic quenching events that occur as H_2O_2 molecules are emitted from individual human epidermal carcinoma cells stimulated by epidermal growth factor. We show mathematically that such arrays can distinguish between molecules originating locally on the cell membrane from other contributions. We find that epidermal growth factor induces 2 nmol H_2O_2 locally over a period of 50 min. This platform promises a new approach to understanding the signalling of reactive oxygen species at the cellular level.

Historically, hydrogen peroxide (H_2O_2) was thought to have only a deleterious role in cell biology as a toxic metabolic waste product, or as part of the immune respiratory burst in response to microbial invasion[1]. New findings suggest that it is a messenger in normal signalling pathways. It is produced when cells are stimulated with various growth factors, cytokines and other signalling molecules, and is known to activate specific downstream targets[2]. Understanding the role of H_2O_2 and other reactive oxygen species (ROS) is hampered by their low concentration and short lifetime. This has inspired the development of innovative detection probes[3–7], but many of these are still unable to map the entire transient signalling response (on a single-molecule level) over its duration with spatial resolution[6–8].

Our laboratory has pioneered the use of single-walled carbon nanotubes (SWNTs) as fluorescent optical sensors for analytical detection from within living cells and tissues. Recent measurements by others[9] and our own laboratory[10,11] have extended the detection limit down to the single-molecule level by analysing the stochastic quenching of excitons as molecules adsorb to the SWNT surface. Here, we develop an array of such single-molecule sensors selective for H_2O_2 that can image the signalling flux emanating from single, living A431 human epidermal carcinoma cells, in real time and with spatial precision. These arrays can resolve several questions about H_2O_2 generation upon growth factor stimulation, including the membrane-localized production compared to the other contributions, its spatial distribution, and through inhibition experiments, the chemical mechanism of the signal response.

A431 cells over-express the epidermal growth factor receptor (EGFR), which is one of four transmembrane growth factor receptor proteins[12]. EGFR is a 170-kDa glycoprotein with an extracellular receptor domain, a transmembrane domain and an intracellular domain[13]. The extracellular domain is divided into four subdomains: I, II, III and IV, with I and III participating in binding[14] (Fig. 1a). A431 cells[15] express $\sim 1 \times 10^6$ EGFRs per cell, whereas only 4×10^4 to 1×10^5 receptors exist in a non-cancerous cell[16]. Epidermal growth factor[16] (EGF)—a single polypeptide chain of 53 amino-acid residues held together by three disulphide bonds in cysteine—stimulates cell growth, proliferation and differentiation on binding to EGFR[16]. Upon activation by EGF, EGFR undergoes dimerization at the cell membrane[13] and an H_2O_2 signal is generated[17]. The chemical origin of this H_2O_2 signal and its relationship to the remaining cascade is largely unknown.

Recent progress in fluorescent probes has confirmed the generation of H_2O_2 signal in A431 in response to EGF, and has also identified a similar mechanism in neuronal cell signalling[6–8]. Our work differs in its single-molecule detection limit, and infinite photoemission lifetime allows continuous detection over the entire response in real time. The array of single-molecule sensors can mathematically discriminate signals generated at the membrane (near-field) from those originating from the cell interior (far-field), an important property for cell analysis. Mapping shown before and after EGF stimulation of A431 cells and NIH-3T3 murine fibroblast cells in real time informs the chemical mechanism of the signalling cascade.

Selective SWNT sensors map H_2O_2 efflux spatially

An SWNT array is ideally suited for imaging H_2O_2 fluxes from living cells (Fig. 1b), because H_2O_2 binds with a forward ($77.8\ M^{-1}\ s^{-1}$) and reverse ($0.0006\ s^{-1}$) rate constant[10] that allows sensitive detection and that excludes other ROS with long lifetimes. Previously[10], we have shown that 'hidden Markov modelling' can determine forward and reverse rate constants from single-molecule adsorbates on SWNTs. Figure 1c demonstrates the results of application of the technique to several species of interest in this work. Except for nitric oxide (NO), H_2O_2 has the largest forward rate constant of all, indicating that its capture probability is the highest. Protons (H^+) can be detected with a forward rate of $8.1\ M^{-1}\ s^{-1}$, but their reverse rate constant is high ($0.0011\ s^{-1}$)

[1]Department of Chemical Engineering, Massachusetts Institute of Technology, Building 66-566, 77 Massachusetts Ave, Cambridge, Massachusetts 02139-4307, USA, [2]Institute of Inherited Metabolic Disorders, 1st Faculty of Medicine, Charles University in Prague, Czech Republic. *e-mail: strano@mit.edu

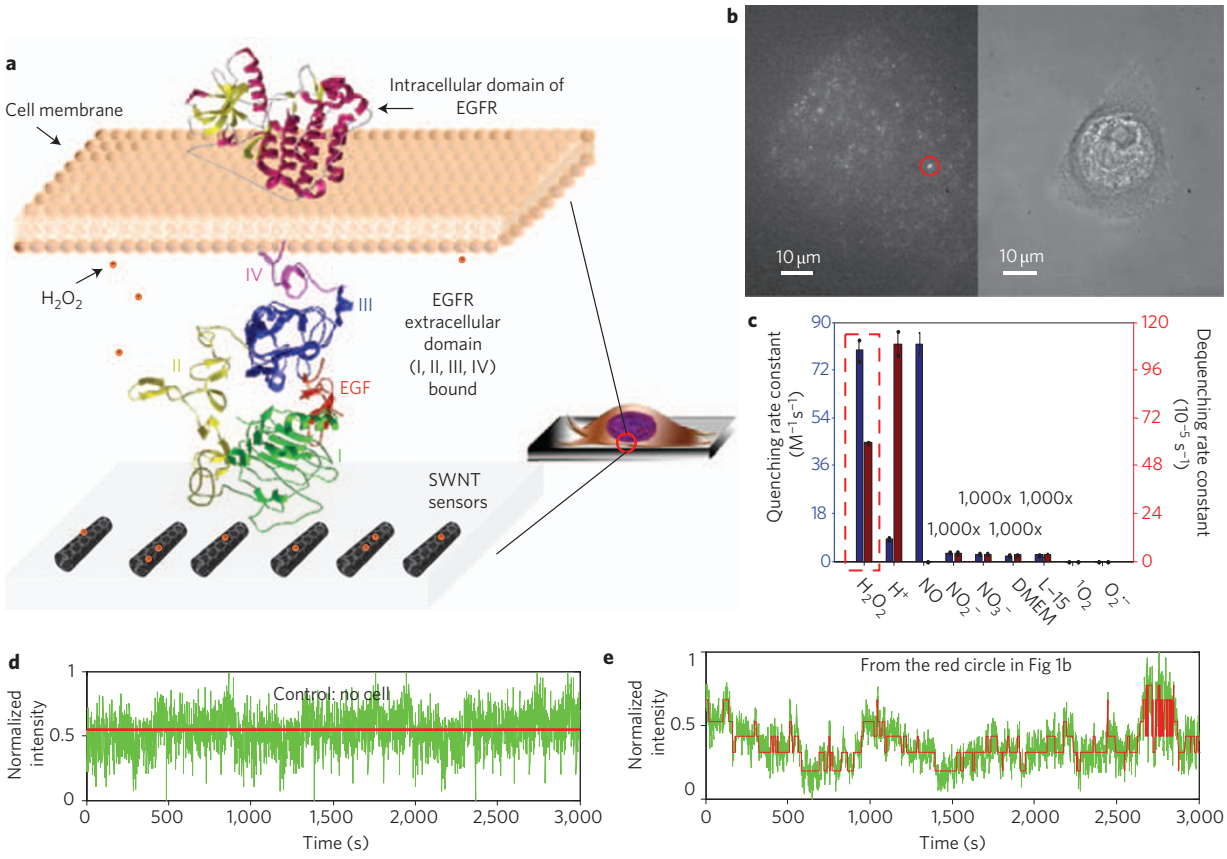

Figure 1 | Nanotube sensing platform. a, A431 cell cultured on a collagen–SWNT film. The enlarged representation of the red circle shows EGFR domains spanning the cell membrane. Domains I and III bind to EGF (red) and generate H_2O_2. **b**, Near-infrared (NIR) image of SWNTs under the A431 (left), and phase contrast image of an A431 cell (right) cultured on SWNT sensors (658 nm excitation, 1 mW, Alpha Plan-Apo ×100/1.46 oil emersion objective). **c**, Forward and reverse binding rates of the SWNT sensor for various analytes show selectivity for H_2O_2. **d**, Fluorescence trace for control (no cells) shows no steps. **e**, Trace for the SWNTs in the red circle in **b** show reversible, stepwise quenching (green trace), modelled by a hidden Markov algorithm (red).

such that, at physiological pH (7.4) their contribution is negligible. Likewise, interfering nitrites and nitrates have small rate constants and there is no contribution from components of cell media. NO has a high forward binding rate of 80.0 M^{-1} s^{-1}, but its reverse rate is almost immeasurable under these experimental conditions. This means that its presence can be easily distinguished, as it irreversibly deactivates the SWNT single-molecule sensor that it encounters. Excluding such signals can subtract the contribution of NO, but no such events were measured in this work, indicating that NO was not detected. In addition, our sensor is inert to singlet oxygen ($^1O_2$) and superoxide ($O_2^{\bullet-}$; Fig. 1c).

Our single-molecule detector array was embedded in a thin film with a roughness of 2 nm (Supplementary Fig. S1) and open porosity (average pore size, 30 nm) towards the SWNTs. Only the most stable species emanating from the cell were therefore detected. For example, $^1O_2$, $O_2^{\bullet-}$ and $OH^{\bullet}$ have lifetimes of 4 μs (ref. 18), 1 μs and 1 ns, respectively[19]. These species are not likely to diffuse into the film and interfere with the SWNTs. The selectivity of our film, together with the diffusion calculation, result in an array of sensors specifically designed to detect single H_2O_2 molecules in real time. We note that this does not limit the approach exclusively to H_2O_2. We recently showed that by varying the chemistry of the encapsulating matrix[20], or by using multiple orthogonal optical responses (multimodality)[11], it is possible to selectively detect virtually any single-molecule analyte emanating from the cell. Future work will support this point.

The detection limit for this class of single-molecule sensor is exchanged for observation time (Supplementary Fig. S2). For example, an array of SWNTs can detect a concentration of 1 μM (10 μM) with an acquisition time of 14 min (3 min).

When no cells are plated onto the collagen–SWNT array, the result is a photoluminescence intensity of constant root-mean-square value. A hidden Markov algorithm finds no quenched states outside the noise floor, as expected. SWNT sensors near or under plated A431 cells show discrete quenching transitions of the type observed previously[9,10]. Stepwise quenching and dequenching reactions are clearly observable (Fig. 1e) when compared to the control experiment (Fig. 1d). Because the collagen–SWNT array has such a high selectivity towards H_2O_2, we assign this flux as single H_2O_2 originating from cellular metabolic activity[2] and also non-specific receptor–ligand binding[21]. To further support this assignment, we use manganese oxide (MnO_2) to selectively catalyse the decomposition of H_2O_2 around the A431 cells both with and without EGF stimulation, to show that the quenching reverses significantly (Supplementary Fig. S3) as H_2O_2 is depleted.

A hidden Markov algorithm was applied to each SWNT signal in the array, yielding the spatial and temporal detection of single molecules emitted from the cell in real time. The typical observation time was 3,000 s, and Fig. 2a–d describes the spatial distribution of detection frequencies for both live (Fig. 2a,b) and fixed (Fig. 2c,d) A431 cells after the addition of EGF (500 ng ml^{-1}) at $t = 0$ using a Matlab program written by us. Each sensor was binned according to its number of quenching transitions within the 3,000 s observation window into one of 16 colour categories between 0 and 150 counts for Fig. 2a–d and between 2 and 70

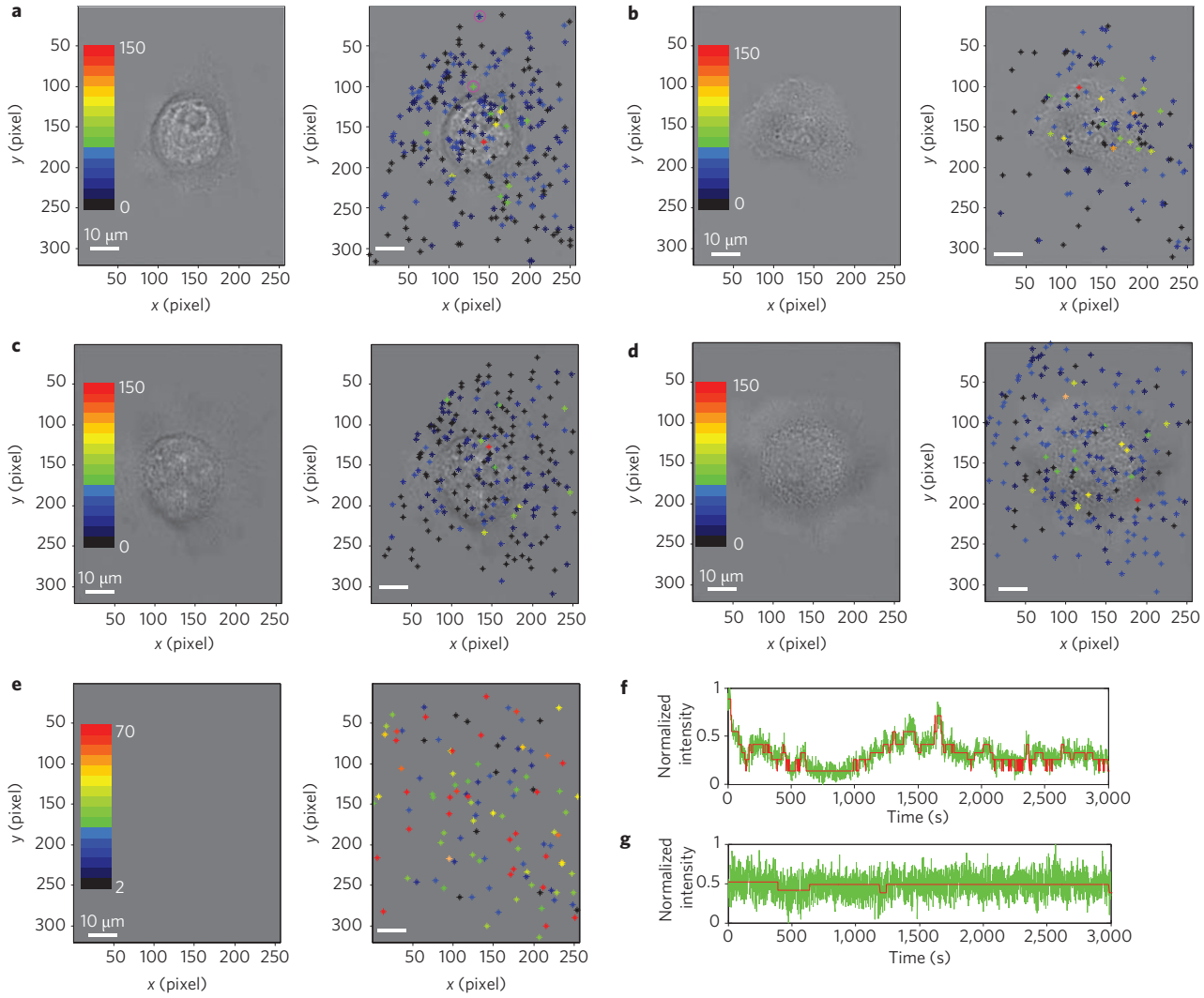

Figure 2 | Spatial mapping of quenching transitions over single A431 cells. a–d, Quenching activity (unit of counts) over the 3,000 s observation window of each sensor, binned into 16 categories represented by 16 different colour bars. Red indicates the highest quenching activity and black the lowest for live (**a**,**b**) and fixed (**c**,**d**) A431 cells. **e**, Control experiment in which 10 μM H_2O_2 was present in the absence of a cell. The left panels show phase contrast images without the overlap of quenching activities. **f**,**g**, Fluorescence traces for nanotubes indicated by the green cross (**f**) and dark blue cross (**g**) in **a**.

counts for Fig. 2e. Note that the control array, exposed to 10 μM H_2O_2 in the absence of cells, demonstrates a spatially random distribution of transition frequencies (Fig. 2e). However, when, instead, A431 cells are present, the frequency distribution possesses a sharp mode invariably confined to the region immediately under the cell. The behaviour is seen for both live and fixed cells. The locations of these 'hotspots' do not remain invariant over the course of the 3,000 s experiment, but shift to alternative regions. The EGFR lifetime[15] is ~30 min, long enough to prevent spatial averaging of the membrane signal. Example fluorescence traces from a nanotube immediately under the cell (green star, highlighted in pink circle, Fig. 2a) and a nanotube far away from the cell (dark blue star, highlighted in pink circle, Fig. 2a) are shown in Fig. 2f and g. It is clear from these examples that the dominant contribution of the H_2O_2 flux comes from the A431 cells, and the data suggest that at any given time it is concentrated at specific locations on the array, unlike the case for a uniformly exposed control.

Real-time quantitative analysis of EGF stimulation

First, we analyse the total dynamic count rate of each single cell in response to EGF to measure the duration of the induced efflux. The quenching rate was calculated in real time for EGF stimulation (500 ng ml^{-1} EGF was added at $t = 0$) on live and fixed 3T3 (Fig. 3a) and A431 cells (Fig. 3b). Compared with the no-cell control and unstimulated cell data, the quenching rates of both A431 and 3T3 cells were increased by EGF stimulation. A431 cells with a higher EGFR density have a much higher quenching rate than 3T3 cells. As can be seen from Fig. 3a,b, the behaviours of single A431 cells after EGF stimulation are similar: the quenching rate increases rapidly immediately after stimulation. However, the time-point of maximal response ranges from 600 to 1,800 s after stimulation. There is no significant difference between live and fixed A431 cells. Removal of EGF decreases the quenching (Supplementary Fig. S4). Compared with ensemble measurements on thousands of cells, our platform allows real-time quantification on single isolated cells. To confirm that the above results correlated with overexpression of EGFR, we then compared the EGFR density in 3T3 cells and A431 cells through immunostaining (see Methods). As can been seen in the confocal images (Fig. 3c,d), A431 cells express much more EGFR than 3T3 cells (see Supplementary Fig. S5 for more immunostaining images). From a calculation on the immunostaining images of 100 cells, the EGFR density of A431 cells is ~10 times that of 3T3 cells, consistent with the literature[15,16].

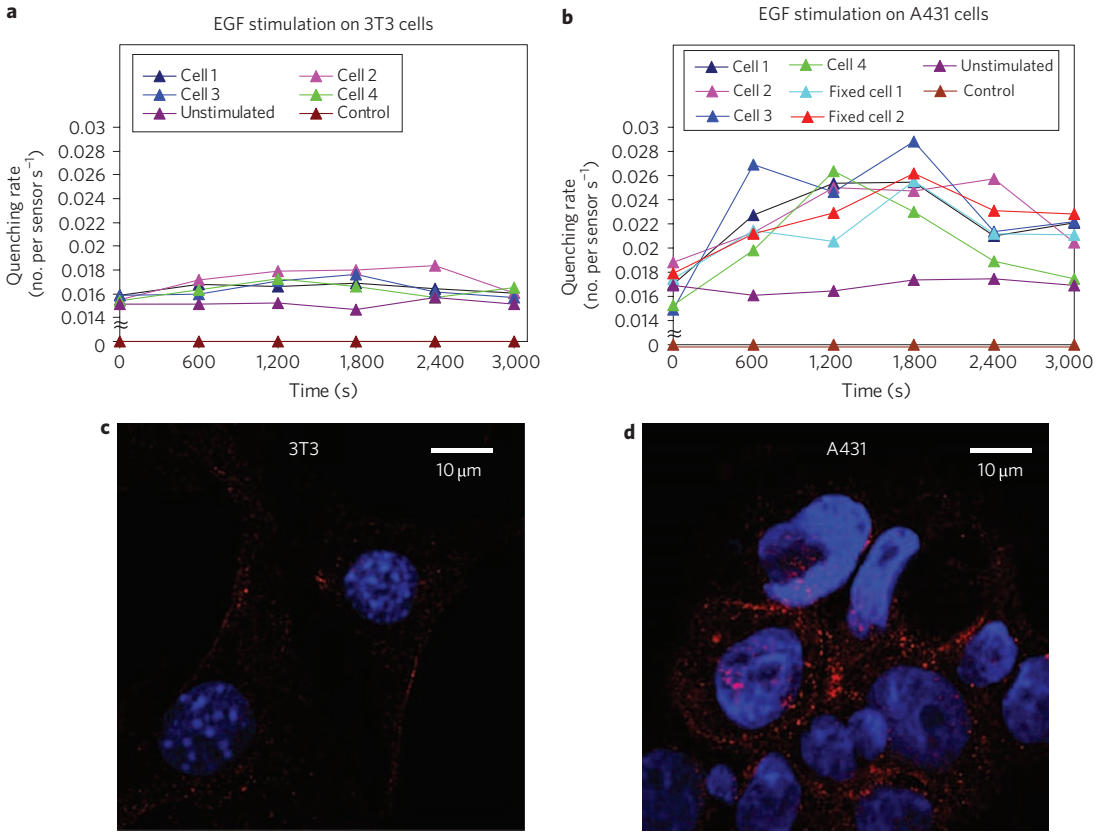

Figure 3 | SWNT quenching depends of EGFR density. a,b, Real-time quenching rate for live 3T3 cells (**a**) and live/fixed A431 cells (**b**). The numbers of sensors under each single cell are 255, 200, 250, 150, 255, 200, respectively, for cells 1, 2, 3, 4, unstimulated, and control (**a**); 160, 110, 126, 174, 140, 180, 180, 200, respectively, for cells 1, 2, 3, 4, fixed cells 1, 2, unstimulated, and control (**b**). **c,d**, Representative confocal images for 3T3 cells (**c**) and A431 cells (**d**) with EGFR (red) labelled with rabbit polyclonal antibody against EGFR and Alexa Fluor 568 donkey anti-rabbit IgG. Nuclei (blue) are stained with 4′,6-diamidino-2-phenylindole (DAPI).

Near-field generation at the membrane

Rank-ordering the sensor responses from lowest to highest capture rates constructs the cumulative distribution (see Supplementary Information). Let x be the number of sensors having a response less than y, so that $x(y)/n$ is then the probability of finding a sensor with a number of counts less than y. For the case of equal capture probabilities, the rank-ordered response is a modified Gamma distribution (Supplementary Fig. S6a,b):

$$x = \frac{n\int_0^y e^{-t}t^{a-1}\mathrm{d}t}{\int_0^\infty e^{-t}t^{a-1}\mathrm{d}t} = \frac{n\Upsilon(a,y)}{\Gamma(a)} = nP(a,y) \qquad (1)$$

where Υ, Γ and P represents the lower incomplete, ordinary and regularized Gamma functions, respectively, with a as the mean value of y.

A kinetic Monte Carlo simulation of 1×10^4 H_2O_2 molecules randomly binned into a sensor array consisting of 300 sensors ($n = 300$) is well described by equation (1) after rank ordering (Supplementary Fig. S6a,b). Note that all the simulations (no fit parameters) used Matlab and were repeated 100 times, with the average reported unless specified otherwise.

An array of sensors capable of detecting discrete, single molecules has the following unique property: it is possible to distinguish between those near-field components generated at the interface and those comprising a far-field component with no memory of origination.

On top of the far-field component described by equation (1), molecules generated near the array surface (that is, at the cell membrane surface) are easily distinguished. The algorithm for extracting this interfacial generation at the interface simply accounts for non-binomial contributions to the frequency distribution. The local response, $y_{\mathrm{local}}(x)$, is given by

$$y_{\mathrm{local}}(x) = y(x) - P^{-1}\left(a, \frac{x}{n}\right) \qquad (2)$$

The mean value a can be found by computing the slope of the experimental data in the $x \to 0$ limit:

$$\frac{\partial y}{\partial x} = \frac{\Gamma(a)}{ny^{a-1}e^{-y}}\left(\text{from } \frac{\partial\Gamma(a,y)}{\partial y} = -y^{a-1}e^{-y}\right)$$

It can be shown from Monte Carlo simulation that membrane generation near the array interface of sufficient activity always biases the rank-ordered response to the highest activity sensors (Fig. 4a,b; see also Supplementary Fig. S6e–i). As a result, a small number of data points at $x \to 0$ are enough to extract the far-field component (equation (1)) from any experimental curve with the membrane generation recovered from equation (2). A practical sensor array constructed as described above has a distribution of sensor capture probabilities as each sensor varies slightly in length and orientation. A beta distribution is a generic, empirical function that can describe this variation. It has the advantage that the far-field component then becomes a cumulative beta binomial distribution (see simulation and fit in Supplementary Fig. S6c,d), and an analogous deconvolution can be derived (Fig. 4c,d). The rank-ordered sensor responses of SWNT–collagen arrays exposed to

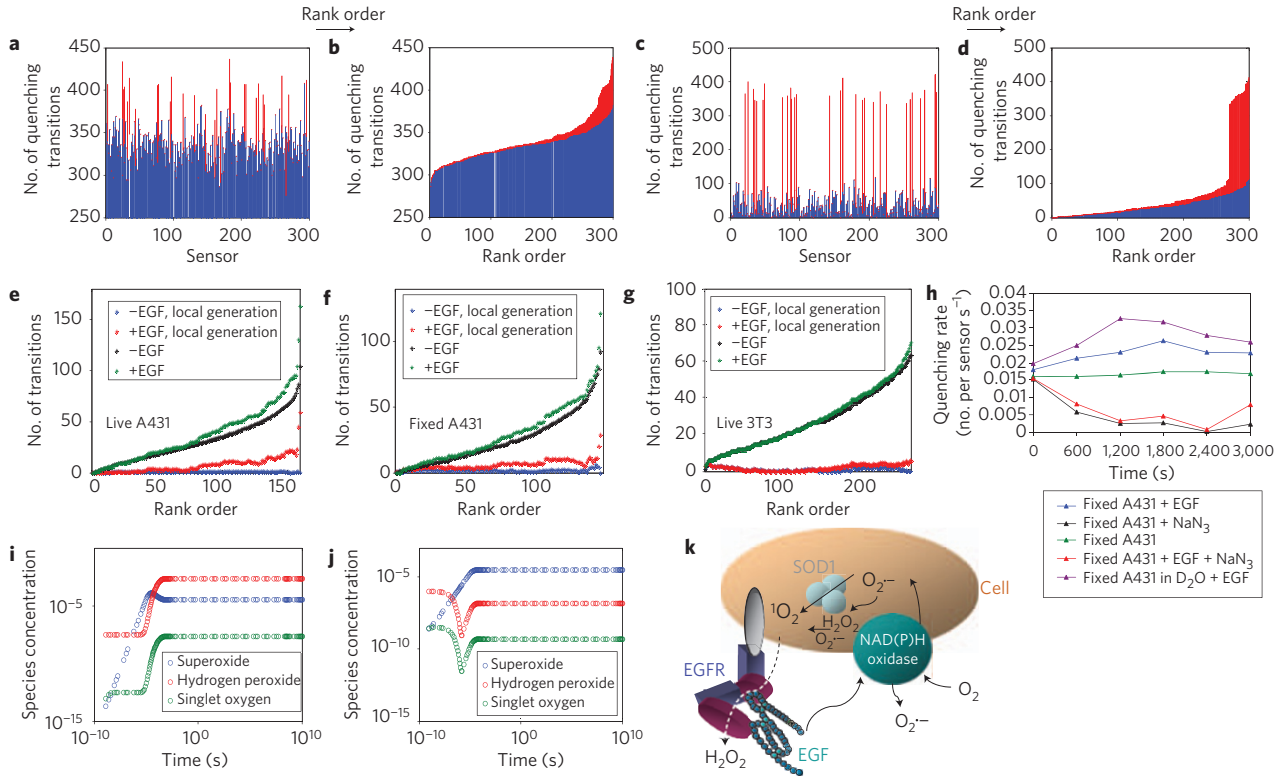

Figure 4 | Quantitative analysis of results from SWNT sensor array. a–d, Simulation of sensor response (**a**), rank-ordered sensor response from **a** (**b**), sensor response following beta distribution (**c**) and rank-ordered sensor response from **c** (**d**) of 1×10^5 H_2O_2 randomly falling onto 300 sensors (blue), with an additional response to local generation (red). **e–g**, Following far-field component subtraction from the rank-ordered sensor response (black, −EGF; green, +EGF), local generation before (blue) and after (red) EGF stimulation for live (**e**) and fixed (**f**) A431 cells and live 3T3 cells (**g**). **h**, Real-time quenching rate for fixed A431, before (green) and after (blue) EGF stimulation. Sodium azide decreases the quenching, with (red) and without (black) EGF. Extending the singlet oxygen lifetime using D_2O increases the quenching (purple). **i,j**, Concentration profiles on a log–log scale for different species from solving reactions (1) to (8) (**i**) and from considering the effect of NaN_3 when solving the reaction network (**j**). **k**, Scheme of the proposed pathway for H_2O_2 generation.

constant (uniform) concentrations of H_2O_2 from 10 to 100 μM are described by beta binomial distributions with parameters $\alpha = 1.2 \pm 0.15$ and $\beta = 3.0 \pm 0.12$ (Supplementary Fig. S7a–d). These parameters were used to correct the measured responses for the variation of capture sensitivities of each SWNT.

Membrane activities on single, live, fixed A431 cells and live 3T3 cells before and after EGF stimulation over 3,000 s were extracted from the above algorithm (Fig. 4e–g; see also Supplementary Fig. S8 for the whole data set). Before stimulation, the local activity is negligible. After stimulation, the membrane generation is observed for both live and fixed A431 cells, but not for live 3T3 cells. The increased activities after stimulation in the unit of number of quenching transitions per sensor are summarized in Table 1. For A431 cells after simulation, the local H_2O_2 concentration is determined through calibration to be 2 μM using control experiments in the cell-free system (Supplementary Fig. S7e). The local generation rate from each membrane source is then 0.04 nmol H_2O_2 min^{-1} (or 2 nmol over a period of 50 min) after correcting for diffusion from Supplementary equation (S3).

A consistent H_2O_2 signal generation mechanism

The spontaneous or catalytic breakdown of $O_2^{\bullet -}$ is considered to be the source of H_2O_2 in many biological pathways, not only for immune cells, but also in a variety of eukaryotic cells[2]. $O_2^{\bullet -}$ can be produced by the partial reduction of oxygen by cytochrome-*c* oxidase in mitochondria[2] or by membrane-associated NAD(P)H oxidase[6]. Extensive literature has shown that EGF-stimulated H_2O_2 generation originates from NAD(P)H oxidase instead of mitochondria for various non-phagocytes, including A431 cells[6,22,23]. Growth factors such as EGF induce the formation of a complex on NAD(P)H oxidase to promote electron transfer from NAD(P)H to molecular oxygen[23]. Fixation of A431 cells using 4% paraformaldehyde was designed to remove the influence of the mitochondria[24] in our experiments, a step that has been used in the literature to kill the cells without affecting the binding abilities of the EGFR[21]. The fact that we see no quantitative difference between live and fixed A431 cells in their EGF-inducible membrane generation (Table 1) is consistent with the existing literature, in which mitochondria do not affect EGF-induced H_2O_2 generation. In addition, our single-molecule sensor array allows the membrane

Table 1 | Number of quenching transitions per sensor from receptors alone, calculated for live and fixed A431 cells and live 3T3 cells.

Cell type	Number of quenching transitions per sensor
Live A431 cell 1	6.6
Live A431 cell 2	4.0
Live A431 cell 3	5.0
Live A431 cell 4	7.5
Fixed A431 cell 1	4.5
Fixed A431 cell 2	7.8
A431 cells average	6.0
Live 3T3 cell 1	1.0
Live 3T3 cell 2	1.1
Live 3T3 cell 3	1.1
Live 3T3 cell 4	1.0
3T3 cells average	1.1

signalling flux to be differentiated from a diffuse far-field component, and can therefore inform the discussion of the nature of the H_2O_2 signal. Our analysis above confirms that the H_2O_2 increase in response to EGF binding is generated at the membrane and not in the cell interior (Fig. 4e–g). It has been demonstrated that H_2O_2 production is EGFR-ligand-dependent in A431 cells[21], the inhibition of EGFR phosphorylation not affecting H_2O_2 generation. At this point, both the signalling network post-NAD(P)H oxidation, and the connection between activation of NAD(P)H oxidase and EGFR-ligand-dependent generation, are unclear from the literature. We further performed an inhibition experiment using NAD(P)H oxidase inhibitors (Supplementary Fig. S9a,b) and an EGFR inhibitor (Supplementary Fig. S9c) and found that, consistent with our speculation, NAD(P)H oxidase inhibitors prevent H_2O_2 from forming, but the EGFR inhibitor has no effect on the H_2O_2 produced.

From previous work, it is also not clear what catalytic portion of EGFR may be responsible for membrane H_2O_2 generation[21]. Tryptophan (Trp) is proposed to be responsible for the conversion of $^1O_2$ to H_2O_2 in antibodies[25]. This antibody-mediated process is triggered upon binding of $^1O_2$ to conserved binding sites within the antibody fold[26], where the antibody serves as the catalyst, stabilizing the intermediate (H_2O_3) and directing its conversion to H_2O_2. Trp is present in both EGF[16] (Trp 49, Trp 50) and EGFR[27] (Trp 140, 176, 453, 492; Fig. 1a). If lacking these Trp residues, EGFR does not bind the ligand with high affinity[27]. It is possible that EGFR, on binding with EGF, allows greater access to sites on the receptor itself that catalyse the conversion of $^1O_2$ to H_2O_2. To explore this, 1 mM sodium azide (NaN_3), a scavenger of $^1O_2$ (ref. 28), was added to fixed A431 cells with and without the presence of EGF, and the single-molecule efflux of H_2O_2 was again recorded. Compared to the unstimulated control (green curve, Fig. 4h), NaN_3 greatly diminished both the near- and far-field portions of the H_2O_2 response to EGF (black and red curves, Fig. 4h). We also observed an increase in H_2O_2 after we exchanged water with D_2O (the lifetime of $^1O_2$ in D_2O is 67 μs (ref. 29), a factor of 16 greater than that in water) for the EGF stimulation experiment on fixed A431 cells (purple curve, Fig. 4h), compared to the parallel experiment conducted with water (blue curve, Fig. 4h). In previous studies, the level of H_2O_2 before and after EGF stimulation was not affected when shutting down the mitochondria[22,23]. The fact that we were able to observe an obvious decrease in H_2O_2 level even below the basal level when adding NaN_3 before and after EGF stimulation, and an increase in H_2O_2 level when extending the lifetime of $^1O_2$, supports a complex pathway involving $^1O_2$.

One possible signalling network that may explain this more complex response starts from $O_2^{\bullet -}$, which is produced from the reduction of molecular oxygen by NAD(P)H oxidase in A431 cells (Fig. 4k)[22,26]:

$$\mathrm{NAD(P)H} + 2O_2 \xrightarrow{\text{NAD(P)H oxidase}} \mathrm{NAD(P)^+} + H^+ + 2O_2^{\bullet -}$$

EGF was found to increase the production of $O_2^{\bullet -}$ in A431 cells, and an inhibitor of NAD(P)H oxidase halts this mechanism in a manner that was also mitochondria-independent[22]. This observation, together with the previous known EGF–EGFR-induced NAD(P)H oxidase activation mechanism for EGF-stimulated A431 cells from numerous examples of the literature[6,22,23], and our inhibition experiment results (Supplementary Fig. S9a,b), supports the above reaction. $O_2^{\bullet -}$ can then be decomposed by superoxide dismutase (SOD). It has been found that SOD is a master regulator of growth factor signalling, and the inhibition of SOD1, which is an abundant copper/zinc enzyme found in the cytoplasm, increases the steady-state levels of $O_2^{\bullet -}$ and decreases the levels of H_2O_2 in A431 cells[30]. These reactions are rapid and occur with a diffusion-limited reaction rate:

$$2O_2^{\bullet -} + 2H^+ \xrightarrow{\text{SOD}} {}^1O_2 + H_2O_2 \text{ (ref. 31)}$$

$$2O_2^{\bullet -} + 2H_2O \xrightarrow{\text{SOD}} O_2 + H_2O_2 + 2\,{}^-OH \text{ (ref. 32)}$$

Transition metal ions such as iron or copper can catalyse the reduction of H_2O_2 by $O_2^{\bullet -}$ (refs 33–35).

$$O_2^{\bullet -} + H_2O_2 \xrightarrow{\text{transition metal ions}} {}^1O_2 + {}^{\bullet}OH + OH^-$$

$^1O_2$ can decay to ground-state oxygen. It has been shown that the decay of $^1O_2$ is determined by its interactions with water in the cell and not by interactions with other cell constituents; its decay rate constant is $3 \times 10^5\ s^{-1}$ (ref. 36).

$${}^1O_2 \xrightarrow{\text{water}} O_2$$

Ferrous also reacts with H_2O_2, and is known as the Fenton reaction[37]:

$$Fe^{2+} + H_2O_2 \longrightarrow Fe^{3+} + {}^{\bullet}OH + OH^-$$

$$Fe^{3+} + O_2^{\bullet -} \longrightarrow Fe^{2+} + O_2$$

On EGF stimulation, $^1O_2$ is converted into H_2O_2, catalysed by EGF–EGFR[38,39]:

$$2\,{}^1O_2 + 2H_2O \xrightleftharpoons{\text{EGF–EGFR}} 2H_2O_2 + O_2$$

From solving the proposed pathway numerically (with the initial values for *in vitro* ROS obtained from the literature[40]: superoxide, ~1 nM; H_2O_2, 1 μM; $^1O_2$, ~1 nM) assuming a well-mixed condition and using the methods in previous work[41,42], the concentration of $O_2^{\bullet -}$ and H_2O_2 increases with the addition of EGF (Fig. 4i), consistent with our experimental observations and those of others[6,17,22]. The addition of NaN_3 causes a decrease of H_2O_2 (Fig. 4j), even below the initial value, consistent with our observations in Fig. 4h. Although the pathway that we have proposed here is compelling, future work is necessary to conclusively rule out alternative mechanisms.

Conclusions

In conclusion, an array of SWNT sensors has been used to image the incident flux of H_2O_2 molecules that stochastically absorb and quench the emission with spatial and temporal resolution. Notably, arrays of this type can distinguish between molecules originating near an interface and those with no memory of origination, attributed as the far-field component. The signalling activity of EGFR on single A431 cells has been successfully measured using this sensor array. We find that EGF stimulation induces, on average, 2 nmol H_2O_2 over a period of 50 min in A431 cells. Corresponding inhibition experiments suggest a mechanism in which water oxidizes $^1O_2$ at a catalytic site on the receptor itself, generating H_2O_2 in response to receptor binding. An EGFR-mediated H_2O_2 generation pathway that is consistent with all current and previous findings has been proposed and numerically tested for consistency.

Methods

Suspension of SWNTs in collagen. Single-walled HiPco carbon nanotubes (Rice University) were suspended in type 1 collagen (BD Biosciences) through 1 min probe-tip sonication (1/4-inch tip, 40% amplitude). A mass of 1 mg of SWNTs was used per ml of 3.41 mg ml^{-1} collagen stock in 0.02 M acetic acid for sonication. The mixture was centrifuged for 270 min at 16,300*g* and the pellet discarded, retaining the supernatant for future experiments.

Collagen–SWNT thin films. Collagen–SWNT was diluted with stock collagen (3.41 mg ml^{-1}) to obtain a concentration of 272 mg l^{-1} SWNTs. This solution was diluted to 50 μg ml^{-1} collagen with 0.02 M acetic acid with a final concentration of SWNTs of 8 mg l^{-1} for imaging purposes (the concentration of SWNTs was found by trial and error to achieve a desirable coverage of SWNTs on the film) and pipetted onto glass-bottomed 35-mm Petri dishes (MatTek Corporation, P35G-1.5-14-C) in 500-μl aliquots to completely cover the glass region in the centre of the dish. The collagen was dried at room temperature in a laminar flow hood. The dried film was rinsed well with phosphate buffer saline (PBS) to remove the remaining acid. Everything was done under a sterilized environment.

Singlet oxygen and superoxide generation. Rose Bengal was used to generate singlet oxygen and superoxide in real time using a procedure described from a previous study[43]. Briefly, 50 nM of rose Bengal was illuminated at 561 nm at 200 mW for 30 min and the fluorescence of nanotubes under this illumination was recorded in real time. It is reported that this procedure will generate both singlet oxygen and superoxide. MnO_2 was added to the solution to prevent any interference from H_2O_2.

Fluorescence microscopy on live and fixed cells. Human epidermoid carcinoma A431 cells and murine NIH-3T3 cells were cultured with Dulbecco's Modified Eagle's Medium (DMEM, ATCC) supplemented with 10% fetal bovine serum (FBS, Gemini Bio-Products) and 1% Pen-Strep Solution (10,000 U ml^{-1} Penicillin-G 10,000 μg ml^{-1} Streptomycin Penicillin–Streptomycin Solution, Gemini Bio-Products) at 37 °C with 5% CO_2 on a collagen film[10] in a glass-bottomed 35-mm Petri dish (MatTek, P35G-1.5-14-C) after serum starvation[17]. Immediately before imaging, the cell medium was changed into Leibovitz's L-15 medium, which buffers the pH in the atmosphere. The nanotubes in the collagen film beneath the cells were then imaged using a fluorescence microscope (Carl Zeiss, Axiovert 200), with a charge-coupled device (CCD) camera (Carl Zeiss, ZxioCam MRm) and two-dimensional InGaAs array (Princeton Instruments OMA 2D). Movies were acquired using the WinSpec data acquisition program (Princeton Instruments). The nanotubes were excited by a 658-nm laser (LDM-OPT-A6-13, Newport Corporation) at 35 mW. After a stable fluorescence intensity was observed (Supplementary Fig. S1), 500 μl of each reagent was added to reach the desirable final concentration. For the experiment with fixed cells, A431 cells were washed with PBS, fixed in 4% paraformaldehyde (pH 7.4) for 10 min, washed three times and were then ready for imaging.

Fluorescent staining of cells. Cells were incubated with 4% PFA/PBS (USB Corporation) at 4 °C for 5 min, at room temperature for 10 min, then with 100% methanol (Sigma) at −20 °C for 10 min. The fixed cells were washed three times with PBS (Hyclone), permeabilized with 0.1% Triton X 100 (Sigma)/PBS for 20 min at room temperature, followed by further washing with PBS. The cells were then incubated in 1% FBS/0.05% Tween (Sigma)-20/PBS for 20 min at room temperature, after which they were incubated with the primary antibody (rabbit polyclonal to EGFR, ABCAM) in 1% FBS/0.05% Tween-20/PBS for 1 h at room temperature. Washing and blocking were repeated. In the dark, the secondary antibody (Alexa Fluor 568 donkey anti-rabbit IgG, Invitrogen) was added in 1% FBS/0.05% Tween-20/PBS for 1 h at room temperature (Alexa 1:500), after which 4',6-diamidino-2-phenylindole (DAPI, Sigma Aldrich) was added with a final concentration of 1 μg l^{-1}. The washing step was repeated. The sample was then mounted in Moviol (Shandon Immu-Mount, Thermo Fisher Scientific). The samples were then analysed using a Zeiss LSM 510 Meta confocal microscope using the same configuration and processed in LSM image Browser software from Zeiss.

Atomic force microscope. An MFP-3D (Asylum Research) was used to carry out tapping-mode atomic force microscopy (AFM) imaging. Samples were directly deposited on a 75 mm × 25 mm glass slide (VWR International) and imaged using rectangular silicon tips (Olympus AC240TS) with a nominal spring constant of 2 N m^{-1}. Both topographic and height images were recorded during AFM analysis. Height analysis was performed using Igor Pro software.

Received 3 September 2009; accepted 27 January 2010; published online 7 March 2010

References

1. Imlay, J. A. Cellular defenses against superoxide and hydrogen peroxide. *Annu. Rev. Biochem.* **77,** 755–776 (2008).
2. Veal, E. A., Day, A. M. & Morgan, B. A. Hydrogen peroxide sensing and signaling. *Mol. Cell* **26,** 1–14 (2007).
3. Belousov, V. V. *et al.* Genetically encoded fluorescent indicator for intracellular hydrogen peroxide. *Nature Methods* **3,** 281–286 (2006).
4. Casanova, D. *et al.* Single europium-doped nanoparticles measure temporal pattern of reactive oxygen species production inside cells. *Nature Nanotech.* **4,** 581–585 (2009).
5. Lee, D. *et al. In vivo* imaging of hydrogen peroxide with chemiluminescent nanoparticles. *Nature Mater.* **6,** 765–769 (2007).
6. Miller, E. W., Tulyanthan, O., Isacoff, E. Y. & Chang, C. J. Molecular imaging of hydrogen peroxide produced for cell signaling. *Nature Chem. Biol.* **3,** 263–267 (2007).
7. Zhou, M., Diwu, Z., Panchuk-Voloshina, N. & Haugland, R. P. A stable nonfluorescent derivative of resorufin for the fluorometric determination of trace hydrogen peroxide: applications in detecting the activity of phagocyte NADPH oxidase and other oxidases. *Anal. Biochem.* **253,** 162–168 (1997).
8. Hong, Y., Blackman, N. M. K., Kopp, N. D., Sen, A. & Velegol, D. Chemotaxis of nonbiological colloidal rods. *Phys. Rev. Lett.* **99,** 178103 (2007).
9. Cognet, L. *et al.* Stepwise quenching of exciton fluorescence in carbon nanotubes by single-molecule reactions. *Science* **316,** 1465–1468 (2007).
10. Jin, H., Heller, D. A., Kim, J.-H. & Strano, M. S. Stochastic analysis of stepwise fluorescence quenching reactions on single-walled carbon nanotubes: single molecule sensors. *Nano Lett.* **8,** 4299–4304 (2008).
11. Heller, D. A. *et al.* Multimodal optical sensing and analyte specificity using single-walled carbon nanotubes. *Nature Nanotech.* **4,** 114–120 (2009).
12. Yarden, Y. & Sliwkowski, M. X. Untangling the ErbB signalling network. *Nature Rev. Mol. Cell Biol.* **2,** 127–137 (2001).
13. Herbst, R. S. Review of epidermal growth factor receptor biology. *Int. J. Radiat. Oncol. Biol. Phys.* **59,** 21–26 (2004).
14. Lax, I. *et al.* Functional-analysis of the ligand-binding site of EGF-receptor utilizing chimeric chicken human receptor molecules. *EMBO J.* **8,** 421–427 (1989).
15. Masui, H., Castro, L. & Mendelsohn, J. Consumption of EGF by A431 cells—evidence for receptor recycling. *J. Cell Biol.* **120,** 85–93 (1993).
16. Carpenter, G. & Cohen, S. Epidermal growth-factor. *Annu. Rev. Biochem.* **48,** 193–216 (1979).
17. Bae, Y. S. *et al.* Epidermal growth factor (EGF)-induced generation of hydrogen peroxide—role in EGF receptor-mediated tyrosine phosphorylation. *J. Biol. Chem.* **272,** 217–221 (1997).
18. Foote, C. S. *Free Radicals in Biology* (Pryor, W. A., ed.) 85–133 (Academic, 1976).
19. Ziyatdinova, G. K., Gil'metdinova, D. M. & Budnikov, G. K. Reactions of superoxide anion radical with antioxidants and their use in voltammetry. *J. Anal. Chem.* **60,** 49–52 (2005).
20. Kim, J.-H. *et al.* The rational design of nitric oxide selectivity in single-walled carbon nanotube near infrared fluorescence sensors for biological detection. *Nature Chem.* **1,** 473–481 (2009).
21. DeYulia, G. J., Carcamo, J. M., Borquez-Ojeda, O., Shelton, C. C. & Golde, D. W. Hydrogen peroxide generated extracellularly by receptor–ligand interaction facilitates cell signaling. *Proc. Natl Acad. Sci. USA* **102,** 5044–5049 (2005).
22. Morazzani, M. *et al.* Monolayer versus aggregate balance in survival process for EGF-induced apoptosis in A431 carcinoma cells: implication of ROS-P38 mapk-integrin A2B1 pathway. *Int. J. Cancer* **110,** 788–799 (2004).
23. Park, H. S. *et al.* Sequential activation of phosphatidylinositol 3-kinase, beta Pix, Rac1, and Nox1 in growth factor-induced production of H_2O_2. *Mol. Cell. Biol.* **24,** 4384–4394 (2004).
24. Ramey, N. A., Park, C. Y., Gehlbach, P. L. & Chuck, R. S. Imaging mitochondria in living corneal endothelial cells using autofluorescence microscopy. *Photochem. Photobiol.* **83,** 1325–1329 (2007).
25. Welsher, K., Liu, Z., Daranciang, D. & Dai, H. Selective probing and imaging of cells with single walled carbon nanotubes as near-infrared fluorescent molecules. *Nano Lett.* **8,** 586–590 (2008).
26. Nieva, J. & Wentworth, P. The antibody-catalyzed water oxidation pathway—a new chemical arm to immune defense? *Trends Biochem. Sci.* **29,** 274–278 (2004).
27. Carpenter, G. *The EGF Receptor Family: Biologic Mechanisms and Role in Cancer* 33–60 (Academic Press, 2003).
28. Harbour, J. R. & Issler, S. L. Involvement of the azide radical in the quenching of singlet oxygen by azide anion in water. *J. Am. Chem. Soc.* **104,** 903–905 (1982).
29. Kuimova, M. K., Yahioglu, G. & Ogilby, P. R. Singlet oxygen in a cell: spatially dependent lifetimes and quenching rate constants. *J. Am. Chem. Soc.* **131,** 332–340 (2009).
30. Juarez, J. C. *et al.* Superoxide dismutase 1 (SOD1) is essential for H_2O_2-mediated oxidation and inactivation of phosphatases in growth factor signaling. *Proc. Natl Acad. Sci. USA* **105,** 7147–7152 (2008).
31. Yang, J. L., Wang, L. C., Chang, C. Y. & Liu, T. Y. Singlet oxygen is the major species participating in the induction of DNA strand breakage and 8-hydroxydeoxyguanosine adduct by lead acetate. *Environ. Mol. Mutagen.* **33,** 194–201 (1999).
32. Fridovich, I. Biology of oxygen radicals. *Science* **201,** 875–880 (1978).
33. Imlay, J. A., Chin, S. M. & Linn, S. Toxic DNA damage by hydrogen peroxide through the fenton reaction *in vivo* and *in vitro*. *Science* **240,** 640–642 (1988).
34. Halliwell, B. & Aruoma, O. I. DNA damage by oxygen-derived species—its mechanism and measurement in mammalian systems. *FEBS Lett.* **281,** 9–19 (1991).
35. Khan, A. U. & Kasha, M. Singlet molecular-oxygen in the Haber–Weiss reaction. *Proc. Natl Acad. Sci. USA* **91,** 12365–12367 (1994).
36. Hatz, S., Lambert, J. D. C. & Ogilby, P. R. Measuring the lifetime of singlet oxygen in a single cell: addressing the issue of cell viability. *Photochem. Photobiol. Sci.* **6,** 1106–1116 (2007).
37. Hardwick, T. J. The rate constant of the reaction between ferrous ions and hydrogen peroxide in acid solution. *Canadian J. Chem.* **35,** 428–436 (1957).

38. Wentworth, P. *et al.* Antibody catalysis of the oxidation of water. *Science* **293,** 1806–1811 (2001).
39. Wentworth, A. D., Jones, L. H., Wentworth, P., Janda, K. D. & Lerner, R. A. Antibodies have the intrinsic capacity to destroy antigens. *Proc. Natl Acad. Sci. USA* **97,** 10930–10935 (2000).
40. Imlay, J. A. Pathways of oxidative damage. *Annu. Rev. Microbiol.* **57,** 395–418 (2003).
41. Zanthoff, H. & Baerns, M. Oxidative coupling of methane in the gas phase. Kinetic simulation and experimental verification. *Ind. Eng. Chem. Res.* **29,** 2–10 (2002).
42. Zhu, J. Y., Dittmeyer, R. & Hofmann, H. Application of sensitivity analysis to the reduction of a complex kinetic model for the homogeneous oxidative coupling of methane. *Chem. Eng. Proc.* **32,** 167–176 (1993).
43. Mizukawa, H. & Okabe, E. Inhibition by singlet molecular oxygen of the vascular reactivity in rabbit mesenteric artery. *Br. J. Pharmacol.* **121,** 63–70 (1997).

Acknowledgements

M.S.S is grateful for a Beckman Young Investigator Award and a National Science Foundation (NSF) Career Award. This work was funded under the NSF Nanoscale Interdisciplinary Research Team on single-molecule detection in living cells using carbon nanotube optical probes. Part of this work was supported by the national grants Ministry of Education of the Czech Republic project no. MSM0021620806 and KAN grant no. 400100701. The authors thank S. Tannenbaum, G.Wogan and L. Trudel and acknowledge a seed grant from the Center for Environmental Health Sciences at MIT. We also thank M. Balastik at Harvard Medical School for assistance with the confocal experiments, K.D. Wittrup, G. Stephanopoulos, J.-H. Ahn, J.-H Han at Chemical Engineering at MIT, S. Sheffield, Mathematics Department, MIT, and Y. Li at University of Illinois Urbana Champaign for helpful discussions.

Author contributions

H.J. and M.S. conceived the experiments, derived the models and wrote the manuscript. H.J. performed the experiments and analysed the data. D.H., M.K., J.-H.K., J.Z. and A.B. all assisted in the experiments. H.J. and M.S. co-wrote the paper with input from N.M.

Additional information

The authors declare no competing financial interests. Supplementary information accompanies this paper at www.nature.com/naturenanotechnology. Reprints and permission information is available online at http://npg.nature.com/reprintsandpermissions/. Correspondence and requests for materials should be addressed to M.S.S.